Jurnal Penelitian Fisika dan Aplikasinya (JPFA) *Volume 10, Issue 02, December 2020*
p-ISSN: 2087-9946 DOI: 10.26740/jpfa.v10n2.p114-124
e-ISSN: 2477-1775 https://journal.unesa.ac.id/index.php/jpfa

Research Article

Analysis of Tsunami Inundation due in Pangandaran Tsunami Earthquake in South Java Area Based on Finite Faults Solutions Model

Ramadhan Priadi [1,a,*], Dede Yunus [1,b], Berlian Yonanda Andrianto [1,c], and Relly Margiono [1,d]

[1] Badan Meteorologi Klimatologi dan Geofisika
Jl. Perhubungan 2, South Tangerang 15221, Indonesia

e-mail: [a] ramadhanpriadi6@gmail.com, [b] dedeyns@gmail.com, [c] yonanda22@gmail.com,
and [d] relly.margiono@stmkg.ac.id
* Corresponding Author

Abstract

On July 17, 2006 an earthquake with a magnitude of M_w 7.7 triggered a tsunami that struck 500 km of the coast in the south of the island of Java. The tsunami generated is classified as an earthquake tsunami because the waves generated were quite large compared to the strength of the earthquake. The difference in the strength of the earthquake and the resulting tsunami requires a tsunami modeling study with an estimated fault area in addition to using aftershock and scaling law. The purpose of this study is to validate tsunamis that occur based on the estimation of the source mechanism and the area of earthquake faults. Determination of earthquake source mechanism parameters using the Teleseismic Body-Wave Inversion method that uses teleseismic waveforms with the distance recorded waveform from the source between 30^0 and 90^0. Whereas, tsunami modeling is carried out using the Community Model Interface for Tsunami (commit) method. Fault plane parameters that obtained were strike 290^0, dip 10^0, and rake 102^0 with dominant slip pointing up to north-north-west with a maximum value of 1.7 m. The fault plane is estimated to have a length of 280 km in the strike direction and a width of 102 km in the dip direction. From the results of the tsunami modeling, the maximum inundation area is 0.32 km^2 in residential areas flanked by Pangandaran bays and the maximum run-up of 380.96 cm in Pasir Putih beach area. The tsunami modeling results in much smaller inundation and run-up from field observations, it was assumed that the fault plane segmentation had occurred due to the greater energy released than the one from the fault area, causing waves much larger than the modeling results.

Keywords: *Tsunami; inundation; run up; source mechanism; tsunami earthquake*

Analisa Inundasi Tsunami Di Selatan Jawa Berdasarkan Solusi Model *Finite Fault*

Abstrak

Pada tanggal 17 Juli 2006 terjadi gempa bumi dengan magitudo M_w 7.7 yang memicu tsunami yang menerjang 500 km wilayah pesisir pantai di selatan pulau Jawa. Tsunami yang ditimbulkan tergolong tsunami earthquake karena gelombang yang ditimbulkan cukup besar dibandingkan dengan kekuatan gempanya. Perbedaan kekuatan gempa dan tsunami yang ditimbulkan memerlukan kajian pemodelan tsunami dengan estimasi luas sesar selain menggunakan aftershock dan scaling law. Tujuan dari penelitian ini yaitu untuk memvalidasi tsunami yang terjadi berdasarkan hasil estimasi mekanisme

sumber dan luas bidang sesar gempabumi. Penentuan parameter mekanisme sumber gempa menerapkan metode Teleseismic Body-Wave Inversion yang menggunakan waveform teleseismic dengan jarak rekaman waveform dari sumber antara $30^0 - 90^0$. *Sedangkan pemodelan tsunami dilakukan dengan metode Community Model Interface for Tsunami (commit). Parameter bidang sesar yang diperoleh yaitu strike* 290^0, *dip* 10^0, *dan rake* 102^0 *dengan slip dominan mengarah ke atas arah utara barat laut dengan nilai maksimum sebesar 1,7 m. Bidang sesar diestimasikan memiliki panjang 280 km pada arah strike dan lebar 102 km pada arah dip. Dari hasil pemodelan tsunami didapatkan wilayah inundasi maksimal 0,32 km^2 di pemukiman penduduk yang diapit oleh kedua teluk pangandaran dan nilai run-up maksimal yang diperoleh setinggi 380,96 cm di daerah Pantai Pasir Putih. Pemodelan tsunami menghasilkan inundasi dan run up yang jauh lebih kecil dari hasil observasi di lapangan diduga telah terjadi segmentasi bidang sesar akibat energi yang dilepaskan lebih besar dibandingkan luasan bidang sesar yang patah, sehingga menimbulkan gelombang yang jauh lebih besar dari hasil pemodelan.*

Kata Kunci: *Tsunami; inundasi; run up; mekanisme sumber; tsunami earthquake*

PACS: 92.10.hl; 91.30.P-; 91.30.Px

Article History: Received: January 6, 2020 Approved with minor revision: May 23, 2020
Accepted: November 3, 2020 Published: December 31, 2020

How to cite: Priadi R, et al. Analysis of Tsunami Inundation due in Pangandaran Tsunami Earthquake in Shouth Java Area Based on Finite Faults Solutions Model. *Jurnal Penelitian Fisika dan Aplikasinya (JPFA)*. 2020; **10**(2): 114-124 DOI: https://doi.org/10.26740/jpfa.v10n2.p114-124.

I. INTRODUCTION

Java is one of the largest islands in Indonesia with a high index of seismic vulnerability [1]. Tectonically, Java is an island that is affected by the subduction of Indo-Australian plates which goes down to the Eurasian plate. This subduction zone occurs at about 200 km off of the south coast of Java with a velocity of 7 cm per year [2]. One interesting area in Java that worth studying is the West Java geological order. Not only that it is being influenced by world's large plates, West Java region is also influenced by fault structures with east-west direction which most of its fault types are reverse and strike slip fault [3]. Three regional structures that affecting West Java are Cimandiri Fault, Baribis Fault, and Lembang Fault [1].

On July 17, 2006 an earthquake with a magnitude of M_w 7.7 occurred at a depth of 20 km. This earthquake triggered a tsunami that hit along 500km of the southern coast of Java, with a high of run-up about 1 m in Pameungpeuk and 3-8 m in Pangandaran. Estimated fault area in tsunami modeling usually uses aftershock distribution scaling [4]. The weakness of this method is that it is not able to explain the actual fault area because the accurate source mechanism data hasn't been calculated yet.

One way that can be used to determine the source mechanism parameter and area of the fault plane is by using the waveform inversion method and by applying the wells and coppersmith equations [5]. Waveform inversion method that used in this reasearch is the Teleseismic Body-Wave Inversion method [6]. The Teleseismic Body-Wave Inversion method uses P, SH, SV, and PP wave phases together in the inversion process, then a multi-layer structure is used to calculate the responses from the source [7]. The use of teleseismic waves is believed to reduce the effect of local noise, so that signals with low frequencies can be obtained optimally and can maximize the results of interpretation of the

source mechanism [6].

The waveform used in the inversion method is a teleseismic waveform with its distance from the source to the station ranging from 30^0 to 90^0 [8]. Teleseismic waveforms are used in the inversion process because they have good low frequency waves [9]. This is due to waves with high frequencies already attenuated during the wave propagation [10]. The waveform inversion will produce source mechanism parameters, slip distribution, and asperity zones in the fault plane. The highest number of slips and energy is not always obtained in the hypocenter position but rather in the asperity zone [11]. The asperity zone is an area in the fault plane which is interlocked due to surface roughness in two rock plane in rigid contact [12].

The estimation results of the fault area and source mechanism parameters obtained from inversion calculations will be used as input in tsunami modeling so that a more accurate tsunami modeling result is obtained. The method used in tsunami modeling is the Community Model Interface for Tsunami (commit) method. ComMIT is a software designed by NOAA (National Oceanic and Atmospheric Administration) to facilitate users in simulating and handling concerns related to bathymetry and topography problems in tsunami cases [13]. ComMIT uses NOAA's Method of Splitting Tsunami (MOST) which is divided into three stages: the deformation phase, the propagation phase, and the inundation phase [14].

Deformation phase is very dependent on the initial data in the form of the fault area and the fault plane parameters so that it is necessary to improve the estimation of the fault area [15]. It is because the initial conditions that simulate changes in the seabed move due to an earthquake [13]. After going through the deformation stage, the next step is the propagation stage where the modeling using Nonlinear Shallow Water (NSW) wave equations is carried out. From the research of Kanamori [16], tsunami earthquake mechanism are formed as a result of a long rupture period which causes slow deformation under the sea floor. Besides, Murotani, et al. [17] states that the rupture length and the extent of asperity greatly affect the magnitude of the earthquake produced.

In some previous studies [4,6,10], the estimated area of the fracture area uses the relationship between magnitude and earthquake and estimates based on aftershock distribution. However, sometimes the estimation given is not suitable for use in earthquake tsunami modeling. In this research, the estimation of the fault area is carried out using teleseismic body wave inversion to obtain an estimate of the fault area based on source parameters.

Pangandaran Tsunami is a tsunami earthquake which has characteristics with a strength that is not too large but produces a large tsunami. In this study, we carried out tsunami modeling from the Pangandaran earthquake on July 17, 2006 with a magnitude of M_w 7.7. Characterization of earthquake tsunamis in past events is needed to estimate tsunami simulations that are formed from the length of the rupture and the deformation form.

II. METHOD

This study uses waveform data of 2006 Pangandaran earthquake in the southern region of Java. Waveform data is obtained from IRIS (Incorporated Research Institutions for Seismology) which can be accessed freely at https://ds.iris.edu/wilber3/. The focus of the research area is divided into 3 grids, namely grid A: $9{,}82^0$ - $5{,}85^0$ S and $105{,}07^0$ - $109{,}81^0$ E , grid B : $7{,}93^0$ - $7{,}44^0$ S dan $108{,}10^0$ - $108{,}77^0$ E, grid C: Pangandaran Regency coastal area which will be divided into 3 to 4 parts. The grid is the input area for tsunami modeling at the study site.

First of all, the obtained teleseismic waveform will be corrected in the p wave and s wave phases using equation (1). The

correction is used to perform power spectral calculations at all recording seismic stations. Furthermore, computing is done using Green Function by calculating the source function and receiver function using the Haskell matrix [18]. Equations (2) and (3) are equations used for computing the Green Function. The equation was developed by Kikuchi and Kanamori [18].

$$exp\left[2\pi f(t_s^* - t_p^*)\right] \quad (1)$$

$$M_{ij} = \sum_{n=1}^{N_b} a_n M_n \quad (2)$$

$$y_j(t;p) = \sum_{n=1}^{N_b} a_n w_{jm}(t;p) \quad (3)$$

After computing the Green Function, the results of the calculations in the form of synthetic signals will be matched with the observed waveform. The wave fitting will produce the moment tensor element M_n which will be calculated and form a moment tensor element matrix. Furthermore, the fault plane is assumed to have a temporal and spatial slip distribution in each direction in each fault plane that is expanded spatially by equation (4) [19].

$$\Delta\dot{u}_i(x,t) = \sum_{j=1}^{J} P^j \hat{u}_t^j(t)\phi^j(x)f^j(x,t) \quad (4)$$

The unit vector representing the slip direction is denoted by $\hat{u}_t^j(t)$. The slip direction is always parallel to the fault plane and is a function of time. $\phi^j(x)$ is a spatial basis function and $f^j(x,t)$ is a slip time function. Determination of the length and width of the fault plane using the Wells and Coppersmith's (1994) equation in equation (5) and (6).

$$Log\ L = 0{,}58\ M_w - 2{,}42 \quad (5)$$

$$Log\ W = 0{,}41\ M_w - 1{,}61 \quad (6)$$

Then, the tsunami modeling is done using nester grid from the ComMIT software. Nested grid is a method of calculating wave height values in a grid in the leap-frog scheme [20]. The leap-frog scheme is used to solve numerical equations when initial sea level conditions are calculated [21]. From the results of the flux, then sea level value at time $k + 1$ is calculated. The constant K is a grid of flux change in units of time. With the leap-frog scheme, the values of F (flux) on the border grid in the overlap area are used to calculate the grid value in the other areas [22].

Figure 1 shows the nested grid scheme for spatial and time grids. The blue triangle symbol shows the water level while the red circle symbol is fulks.

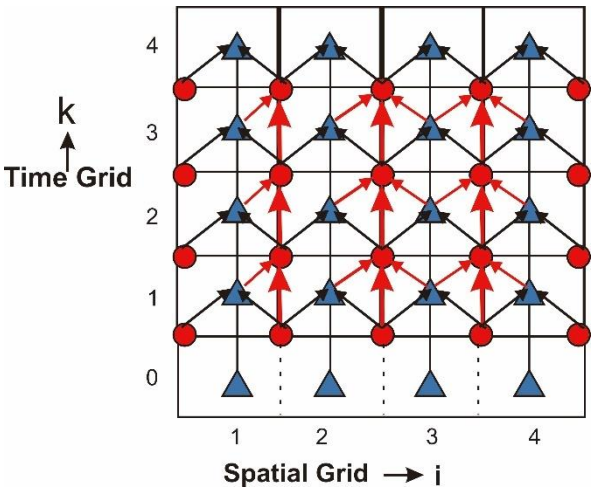

Figure 1. Illustration of Leap-Frog Scheme [20]

In flux grid, the continuity equation is used while the water level grid uses the momentum equation. Equation (7) is a momentum equation and equation (8) is a continuity equation. The equation is a leap-frog scheme developed by Yanagisawa [23]

$$M^{k+\frac{1}{2}} = M^{k-\frac{1}{2}} - gD_{t+\frac{1}{2}}\frac{\Delta t}{\Delta x}(\eta_{t+1} - \eta_t) \quad (7)$$

$$\eta^{k+1} = \eta^k - \frac{\Delta t}{\Delta x}\left(M_{t+\frac{1}{2}} - M_{t-\frac{1}{2}}\right) \quad (8)$$

Tsunami modeling results will produce inland wave height and inundation. The modeling obtained has been corrected by the area of fault and source mechanism parameters from the results of the fault solution.

III. RESULTS AND DISCUSSION

Fault plane parameters obtained from the Pangandaran earthquake are strike 290^0, dip 10^0, and rake 102^0 in nodal 1 whereas in nodal 2 field are strike 98^0, dip 80^0, and rake 88^0 . The Pangandaran area has a strike direction that corresponds to the nodal 1 plane because it leads to a subduction zone in south of Java. Figure 2 shows the results of teleseismic body wave inversions from the Pangandaran M_w 7.7 earthquake.

The results of the comparison between observational waves and synthetic waves produce an error rate (variant) of 0.3675. Moment rate (M_0) of the inversion result is 0.538×10^{21} Nm which is equivalent to the magnitude of M_w 7.62. The wave inversion indicates Pangandaran earthquake has a source time duration of 90 seconds with a maximum peak at 60 seconds.

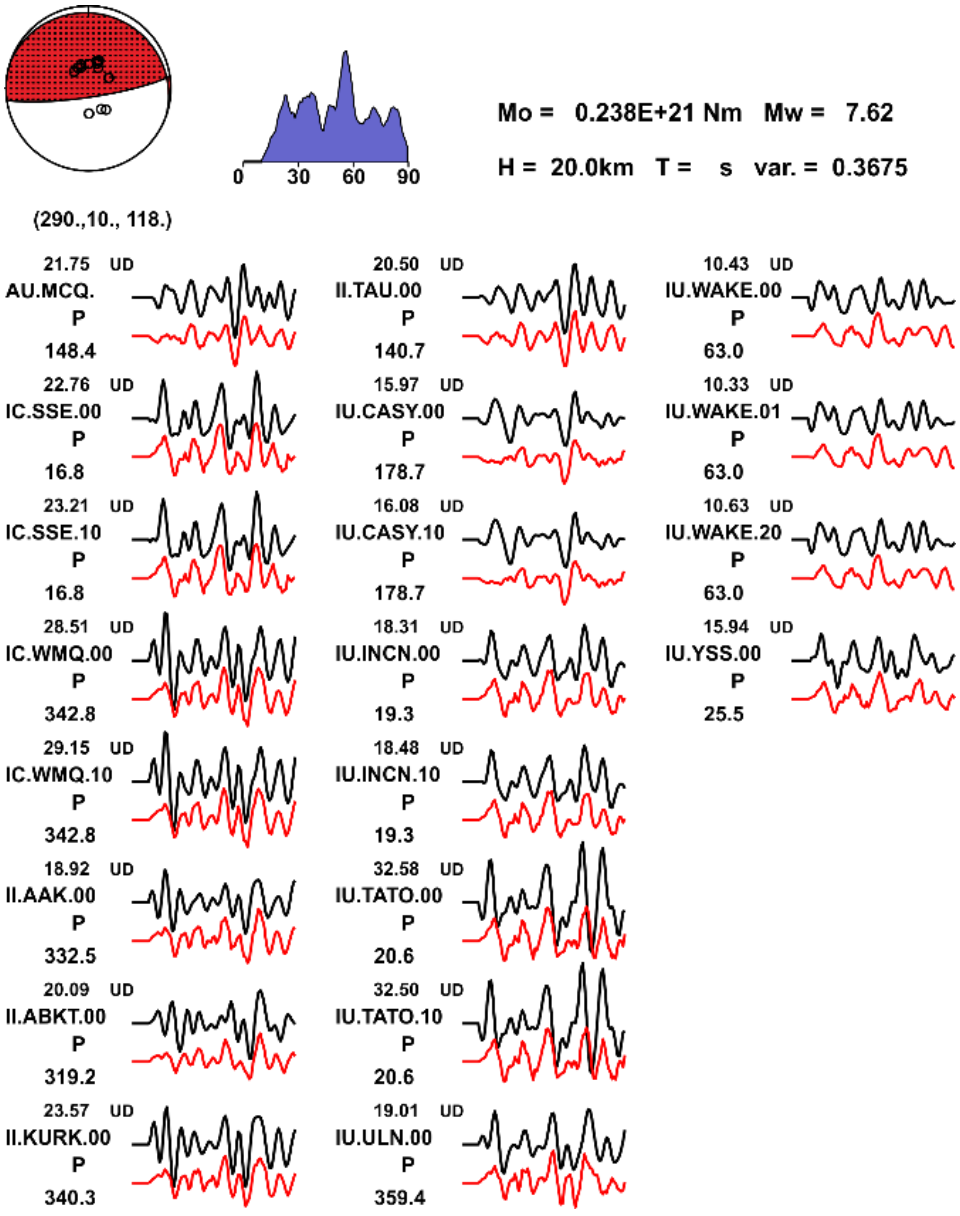

Figure 2. The Result of Body Teleseismic Wave Inversion of 7.7 M_w Pangandaran Earthquake (08:19:26 UTC)

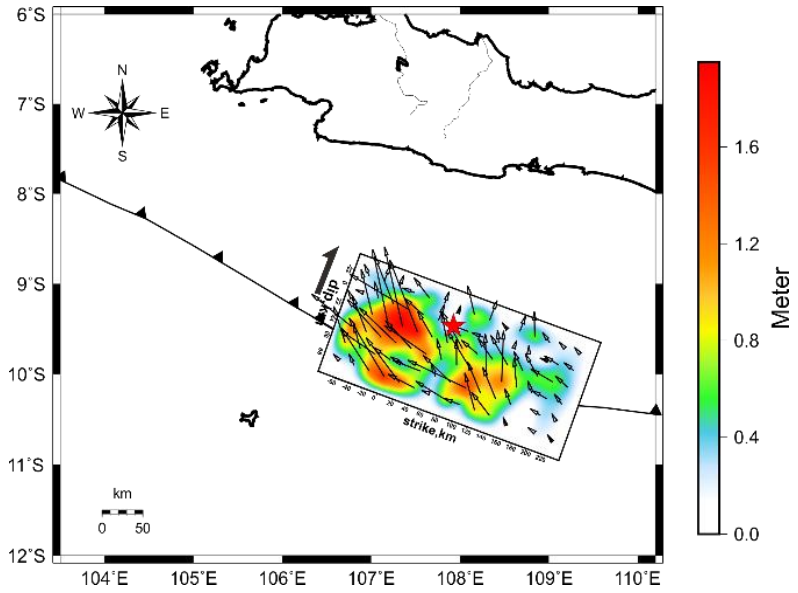

Figure 3. Map of Slip Distribution and Asperity Zones of 7,7 M_w Pangandaran Earthquake

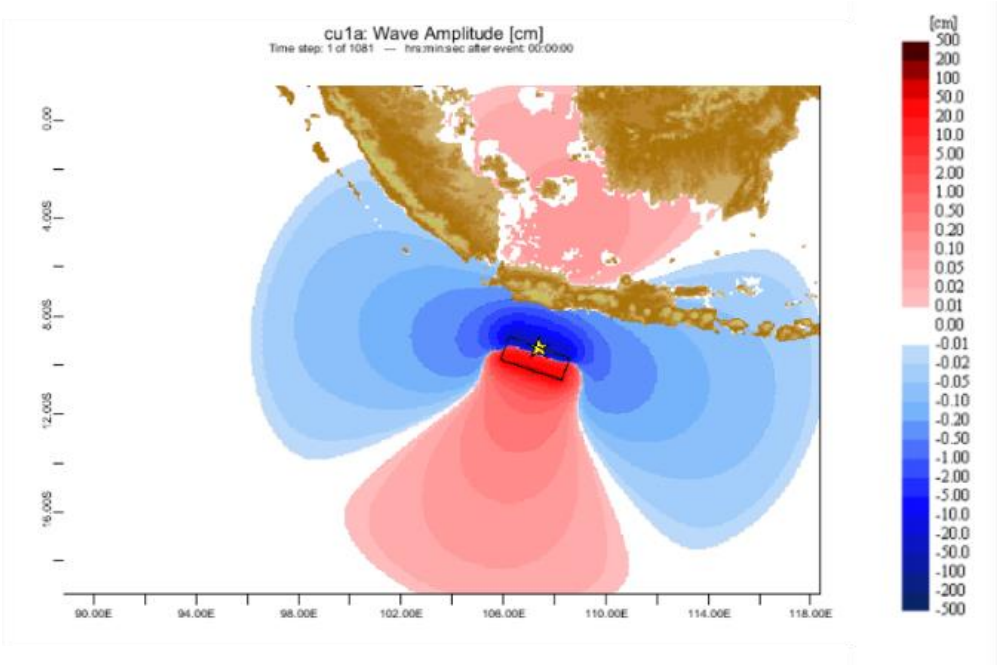

Figure 4. Fault Plane Parameters as Input for ComMIT Tsunami Modeling Scenario

From the obtained plane mechanism, it is known that Pangandaran earthquake is an earthquake with a type of thrust fault with a depth of 20 km. The average seismic wave from the Pangandaran earthquake has a clear initial wave impulse. From the inversion process, the distribution of slip and asperity will be obtained. To clarify the distribution of Pangandaran earthquake slip, orthogonal projection is made to the surface.

Figure 3 shows the map of slip and asperity distribution of Pangandaran earthquake from orthogonal projection results. It shows that the dominant slip is pointing up with north-northwest direction. The maximum slip produced is 1.7 and is located west of the earthquake hypocenter. The width of the fault area from the inversion results is estimated to have a length of 280 km in the strike direction and a width of 102 km in the

dip direction. The area of the fault is divided into 15 × 6 sub-faults with dimensions of 20 km × 22 km for each sub-fault grid in the direction of strike and dip. The map shows that asperity is formed in the down-dip part of the initial break (hypocenter).

The highest number of slips is not always near the initial break but rather in areas with high asperity [24]. Asperity occurs in areas with the least aftershock [25]. There is a large accumulation of stress in the down-dip area, marked by high asperity in the down-dip section. This indicates that there is a strong push from the subduction zone [26]. Asperity formed in the Pangandaran earthquake is not a single asperity, so that cementation can occur to the right and left of the estimated fault area [27]. Fault plane parameters that have been successfully identified are then used as scenario input for tsunami modeling with the ComMIT software.

From the results of the modeling, the height of the sea level in the fault area has increased between 20-40 cm shortly after the earthquake. Figure 4 shows the fault plane parameters obtained as a form of tsunami modeling. The sea waves then propagate and approach the coast with increasing height.

The tsunami arrival time on grid C1 was 48-57 minutes after the earthquake occurred, while on the C2 grid, it was 50-53 minutes after the earthquake occurred. The maximum amplitudes on the C1 and C2 grids are 422.4 cm and 221.9 cm respectively.

Figure 5 shows the initial condition from the Pangandaran tsunami modeling results. Maximum amplitude occurs in the area around Pangandaran Beach and Muara Bojong Salawe. The topography of the study area in a form of a bay is a factor causing the high tsunami waves [27].

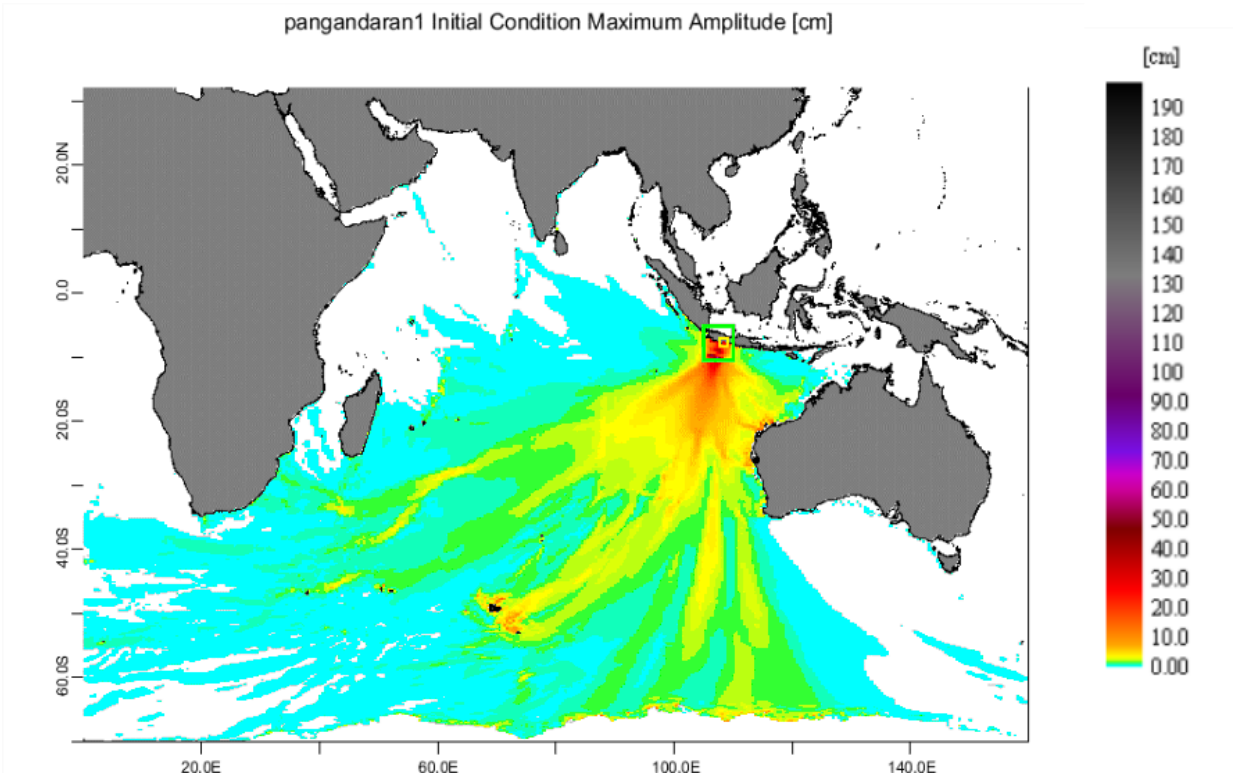

Figure 5. Initial Condition of Pangandaran tsunami modeling

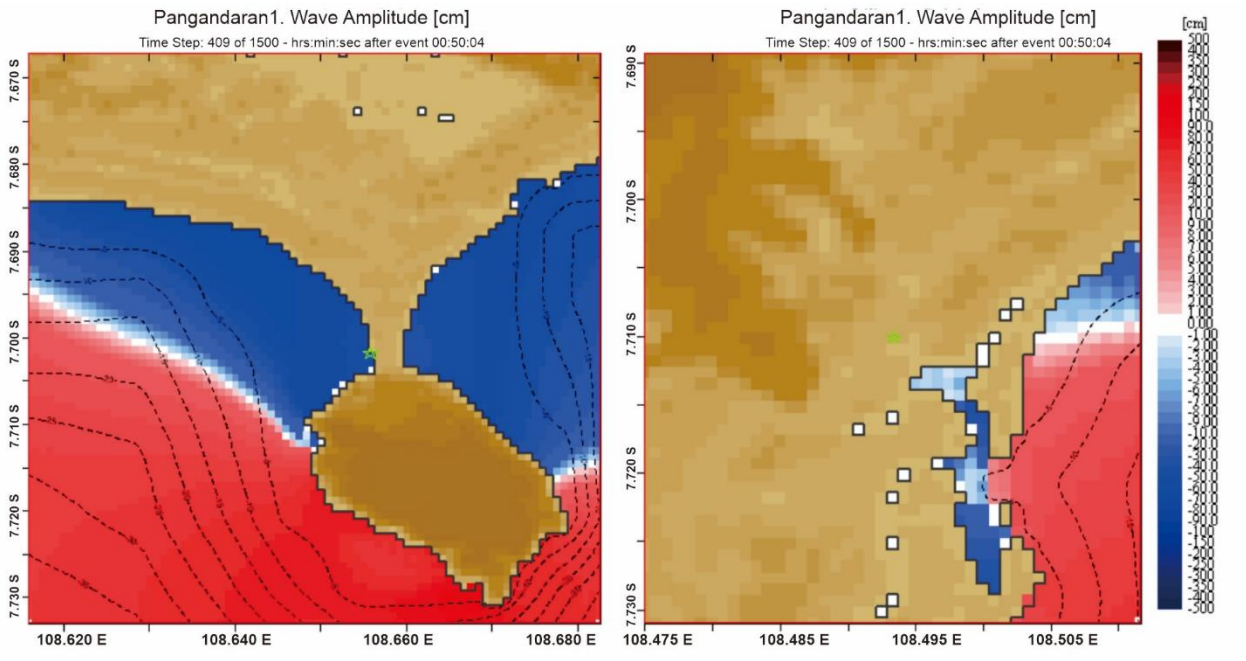

Figure 6. Snapshot of Tsunami Arrival Time at Minute 50 for Grid C1 (Left) and C2 Grid (Right)

From the modeling results, the maximum run-up value is 380.96 cm on the C1 grid (Pantai Pasir Putih area) and 160.62 cm on the C2 grid (west of the Pangandaran airport runway). The results of the modeling are shown in Figure 6. The total area affected in the study area reached 53,894 km^2 on the C1 grid and 18.76 km^2 on the C2 grid. Figure 7 shows the submerged area from the results of the Pangandaran tsunami modeling. The maximum inundation area on the C1 grid is 0.32 km^2 and 0.27 km^2 on the C2 grid.

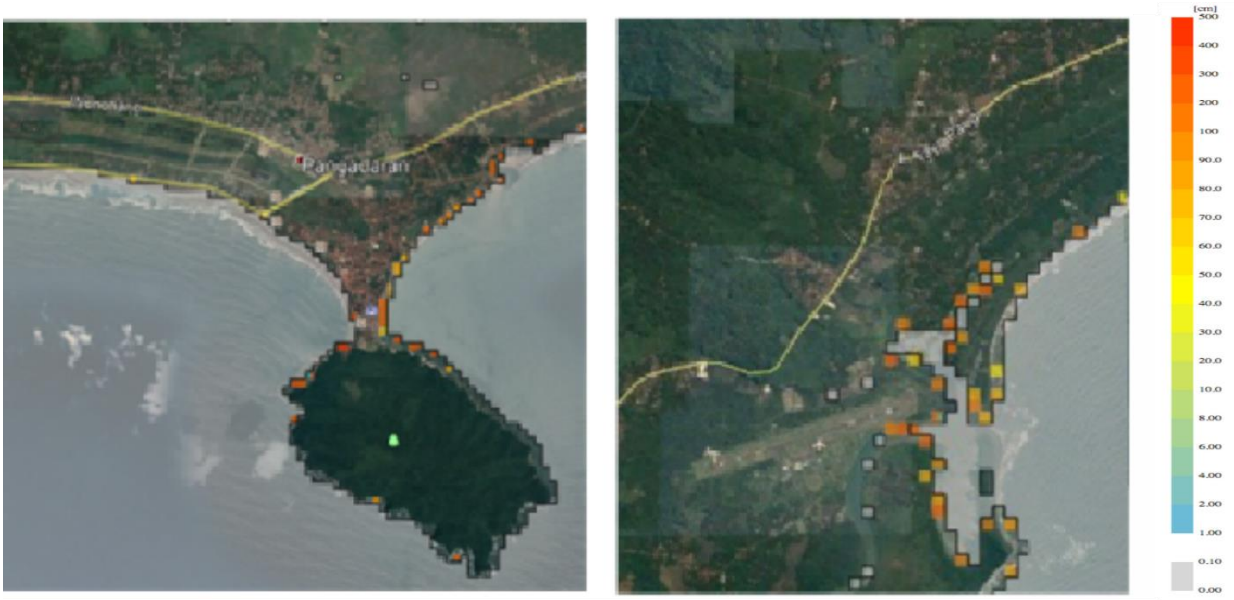

Figure 7. Submerged / inundation area of grid C1 (left) and grid C2 (right)

The area with maximum submergence is in residential areas flanked by both Pangandaran Bay (grid C1) and west of Pangandaran Airport around Muara Bojong Salawe (grid C2). When referring to the results of the research by Yamanaka and

Kikuchi [28] only earthquakes with a single asperity can generate earthquakes that trigger tsunamis when the hypocenter is at sea. Research of Yamanaka and Kikuchi [28] shows that Tokachi-Oki earthquake has the potential to generated a tsunami because it has a single asperity. This is consistent with the obtained inversion results if the Pangandaran earthquake has a single asperity that has the potential to generated a tsunami.

These results indicate the assumption of the fault area is very influential on the results of tsunami modeling [29]. Based on the formed finite asperities modeling results, a large energy accumulation in the down-dip section is seen and it almost covers the entire estimated fault area. It is suspected that in the Pangandaran earthquake, there was a segmentation of the fault plane due to the release of energy greater than the one of the fault area [30]. This causes the rupture to occur longer than the actual fault area because the results of modeling are much smaller than the results of field observations. The earthquake tsunami is a phenomenon that is still debated. The presumption that is always expressed is the occurrence of segmented ruptures so as to provide enough energy to produce a tsunami. This research is expected to provide other options for calculating fault area for tsunami modeling. In addition, this research is expected to be a reference in the field of geophysics.

IV. CONCLUSION

The Pangandaran earthquake is a unique earthquake because it can cause tsunamis even with only moderate magnitude. Finite processing results indicate that the largest slip is pointing up with the north-northwest direction. The maximum inundation area is in the residential areas flanked by both Pangandaran Bay and west of Pangandaran Airport around Muara Bojong Salawe. It is suspected that the Pangandaran earthquake was segmented due to the release of energy which is greater than the fault plane. This caused the Pangandaran earthquake to be accompanied by a tsunami. Improvement in estimated fault area can provide improvements to earthquake tsunami modeling going forward.

REFERENCES

[1] Bird P. An Updated Digital Model of Plate Boundaries. *Geochemistry, Geophysics, Geosystems.* 2003; **4**(3): 1027. DOI: https://doi.org/10.1029/2001GC000252.

[2] Abdurrachman M, Widiyantoro S and Alim MZA. New Model of Wadati-Benioff Zone in Java-Sumatra Subduction System and Its Tectonic Implication. *Conference of the Arabian Journal of Geosciences*. Switzerland: Springer. 2019; 21-24. DOI: https://doi.org/10.1007/978-3-030-01575-6_5.

[3] Haryanto I. Struktur Geologi Paleogen dan Neogen di Jawa Barat. *Bulletin of Scientific Contribution*. 2006; **4**(1): 88-95. Available from: http://jurnal.unpad.ac.id/bsc/article/view/8118.

[4] Negishi H, Mori J, Sato T, Singh RP, Kumar S, and Hirata N. Size and Orientation of the Fault Plane for the 2001 Gujarat, India Earthquake (Mw7. 7) from Aftershock Observations: A High Stress Drop Event. *Geophysical Research Letters*. 2002; **29**(20): 1949. DOI: https://doi.org/10.1029/2002GL015280.

[5] Wells DL and Coppersmith KJ. New Empirical Relationships among Magnitude, Rupture Length, Rupture Width, Rupture Area, and Surface Displacement. *Bulletin of the Seismological Society of America*. 1994; **84**(4): 974-1002. Available from: https://pubs.geoscienceworld.org/ssa/bssa/article-abstract/84/4/974/119792.

[6] Kikuchi M and Kanamori H. *Note on Teleseismic Body-Wave Inversion Program*;

2003. Available from: http://wwweic.eri.u-tokyo.ac.jp/ETAL/KIKUCHI/.

[7] Kikuchi M and Kanamori H. Inversion of Complex Body Waves—III. *Bulletin of the Seismological Society of America*. 1991; **81**(6): 2335-2350. Available from: https://pubs.geoscienceworld.org/ssa/bssa/article-abstract/81/6/2335/102472.

[8] Kikuchi M and Kanamori H. Inversion of Complex Body Waves-II. *Physics of the Earth and Planetary Interiors*. 1986; **43**(3): 205-222. DOI: https://doi.org/10.1016/0031-9201(86)90048-8.

[9] Kikuchi M and Kanamori H. Inversion of Complex Body Waves. *Bulletin of the Seismological Society of America*. 1982; **72**(2): 491–506. Available from: https://pubs.geoscienceworld.org/ssa/bssa/article-abstract/72/2/491/118251.

[10] Lay T and Kanamori H. An Asperity Model of Large Earthquake Sequences. *Earthquakke Prediction – An International Review*. Washington DC: American Geophysical Union; 1981: 579-592. Available from: https://core.ac.uk/reader/33115280.

[11] Yamanaka Y and Kikuchi M. Asperity Map along the Subduction Zone in Northeastern Japan Inferred from Regional Seismic Data. *Journal of Geophysical Research: Solid Earth*. 2004; **109**(B7): B07307. DOI: https://doi.org/10.1029/2003JB002683.

[12] Kikuchi M and Kanamori H. Rupture Process of the Kobe, Japan, Earthquake of Jan. 17, 1995, Determined from Teleseismic Body Waves. *Journal of Physics of the Earth*. 1996; **44**(5): 429-436. DOI: https://doi.org/10.4294/jpe1952.44.429.

[13] Kaiser G, Scheele L, Kortenhaus A, Løvholt F, Römer H, and Leschka S. The Influence of Land Cover Roughness on the Results of High Resolution Tsunami Inundation Modeling. *Natural Hazards and Earth System Sciences*. 2011; **11**(9): 2521-2540. DOI: https://doi.org/10.5194/nhess-11-2521-2011.

[14] Titov VV, Moore CW, Greenslade DJM, Pattiaratchi C, Badal R, Synolakis CE, and Kânoğlu U. A New Tool for Inundation Modeling: Community Modeling Interface for Tsunamis (ComMIT). *Pure and Applied Geophysics*. 2011; **168**: 2121-131. DOI: https://doi.org/10.1007/s00024-011-0292-4.

[15] Borrero JC, Bell R, Csato C, Delange W, Gorong D, Greer SD, Pickett V, and Power W. Observations, Effects and Real Time Assessment of the March 11, 2011 Tohoku-Oki Tsunami in New Zealand. *Pure and Applied Geophysics*. 2013; **170**: 1229-1248. DOI: https://doi.org/10.1007/s00024-012-0492-6.

[16] Kanamori H. Mechanism of Tsunami Earthquakes. *Physics of the Earth and Planetary Interiors*. 1972; **6**(5): 346-359. DOI: https://doi.org/10.1016/0031-9201(72)90058-1.

[17] Murotani S, Satake K and Fujii Y. Scaling Relations of Seismic Moment, Rupture Area, Average Slip, and Asperity Size for M~9 Subduction-zone Earthquakes. *Geophysical Research Letters*. 2013; **40**(19): 5070-5074. DOI: https://doi.org/10.1002/grl.50976.

[18] Haskell NA. The Dispersion of Surface Waves on Multilayered Media. *Bulletin of the Seismological Society of America*. 1953; **43**(1): 17-34. Available from: https://pubs.geoscienceworld.org/ssa/bssa/article-abstract/43/1/17/115661/The-dispersion-of-surface-waves-on-multilayered?redirectedFrom=fulltext .

[19] Kikuchi M, Kanamori H, and Satake K. Source Complexity of the 1988 Armenian Earthquake: Evidence for a Slow After-slip Event. *Journal of Geophysical Research: Solid Earth*. 1993; **98**(B9): 15797-15808. DOI: https://doi.org/10.1029/93JB01568.

[20] Kowalik Z and Murty TS. Numerical Simulation of Two-dimensional Tsunami Runup. *Marine Geodesy*. 1993; **16**(2): 87-

100. DOI: https://doi.org/10.1080/15210609309379681.

[21] Liu PLF, Yeh H, and Synolakis C. *Advance in Coastal and Ocean Engineering Advanced Numerical Models for Simulating Tsunami Waves and Runup*. Singapore: World Scientific Publishing; 2008. DOI: https://doi.org/10.1142/6226.

[22] Zhou H, Moore CW, Wei Y, and Titov VV. A Nested-Grid Boussinesq-Type Approach to Modelling Dispersive Propagation and Runup of Landslide-Generated Tsunamis. *Natural Hazards and Earth System Sciences*. 2011; **11**(10): 2677-2697. DOI: https://doi.org/10.5194/nhess-11-2677-2011.

[23] Sakaizawa H, Aoki A, Sassa K, and Inoue K. Numerical Simulation of 1792 Ariake-Kai Tsunami Using Landslide-Tsunami Model. *Journal of Japan Society Civil Engineers Series B2 (Coastal Engineering)*. 2014; **70**(2): 151-155. DOI: https://doi.org/10.2208/kaigan.70.I_151.

[24] Kikuchi M, Nakamura M, and Yoshikawa K. Source Rupture Processes of the 1944 Tonankai Earthquake and the 1945 Mikawa Earthquake Derived from Low-Gain Seismograms. *Earth, Planets and Space*. 2003; **55**: 159-172. DOI: https://doi.org/10.1186/BF03351745.

[25] Yagi Y, Mikumo T, Pacheco J, and Reyes G. Source Rupture Process of the Tecomán, Colima, Mexico Earthquake of 22 January 2003, Determined by Joint Inversion of Teleseismic Body-Wave and near-Source Data. *Bulletin of the Seismological Society of America*. 2004; **94**(5): 1795-1807. DOI: https://doi.org/10.1785/012003095.

[26] Johnson JM and Satake K. Asperity Distribution of Alaskan-Aleutian Earthquakes: Implications for Seismic and Tsunami Hazards. In Hebenstreit G, *Perspectives on Tsunami Hazard Reduction*. Dordrecht: Springer; 1997: 67–81. DOI: https://link.springer.com/chapter/10.1007%2F978-94-015-8859-1_5.

[27] Merati N, Chamberlin C, Moore C, Titov V, and Vance TC. Integration of Tsunami Analysis Tools into a GIS Workspace–Research, Modeling, and Hazard Mitigation Efforts within NOAA's Center for Tsunami Research, In Showalter P, Lu Y (Eds.), *Geospatial Techniques in Urban Hazard and Disaster Analysis. Geotechnologies and the Environment,* Vol 2. Dordrecht: Springer; 2009: 273-294. DOI: https://doi.org/10.1007/978-90-481-2238-7_14.

[28] Yamanaka Y and Kikuchi M. Source Process of the Recurrent Tokachi-Oki Earthquake on September 26, 2003, Inferred from Teleseismic Body Waves. *Earth, Planets and Space*. 2003; **55**(12): e21-e24. DOI: https://doi.org/10.1186/BF03352479.

[29] Fan W, Bassett D, Jiang J, Shearer PM, and Ji C. Rupture Evolution of the 2006 Java Tsunami Earthquake and the Possible Role of Splay Faults. *Tectonophysics*. 2017; **721**: 143-150. DOI: https://doi.org/10.1016/j.tecto.2017.10.003.

[30] Fukao Y. Tsunami Earthquakes and Subduction Processes near Deep-sea Trenches. *Journal of Geophysical Research: Solid Earth*. 1979; **84**(B5): 2303-2314. DOI: https://doi.org/10.1029/JB084iB05p02303.